AMERICAN SOCIETY FOR MICROBIOLOGY | Infection and Immunity®

CELLULAR MICROBIOLOGY:
PATHOGEN-HOST CELL MOLECULAR INTERACTIONS

# *Neisseria meningitidis* Type IV Pili Trigger $Ca^{2+}$-Dependent Lysosomal Trafficking of the Acid Sphingomyelinase To Enhance Surface Ceramide Levels

**Simon Peters,[a] Jan Schlegel,[b] Jérôme Becam,[a] Elita Avota,[c] Markus Sauer,[b] Alexandra Schubert-Unkmeir[a]**

[a]Institute of Hygiene and Microbiology, University of Wuerzburg, Wuerzburg, Germany
[b]Department of Biotechnology and Biophysics, Biocenter, University of Wuerzburg, Wuerzburg, Germany
[c]Institute for Virology and Immunobiology, University of Wuerzburg, Wuerzburg, Germany

**ABSTRACT** Acid sphingomyelinase (ASM) is a lipid hydrolase that converts sphingomyelin to ceramide and that can be activated by various cellular stress mechanisms, including bacterial pathogens. Vesicle transportation or trafficking of ASM from the lysosomal compartment to the cell membrane is a prerequisite for its activation in response to bacterial infections; however, the effectors and mechanisms of ASM translocation and activation are poorly defined. Our recent work documented the key importance of ASM for *Neisseria meningitidis* uptake into human brain microvascular endothelial cells (HBMEC). We clearly identified OpcA to be one bacterial effector promoting ASM translocation and activity, though it became clear that additional bacterial components were involved, as up to 80% of ASM activity and ceramide generation was retained in cells infected with an *opcA*-deficient mutant. We hypothesized that *N. meningitidis* might use pilus components to promote the translocation of ASM into HBMEC. Indeed, we found that both live, piliated *N. meningitidis* and pilus-enriched fractions trigger transient ASM surface display, followed by the formation of ceramide-rich platforms (CRPs). By using indirect immunocytochemistry and direct stochastic optical reconstruction microscopy, we show that the overall number of CRPs with a size of ~80 nm in the plasma membrane is significantly increased after exposure to pilus-enriched fractions. Infection with live bacteria as well as exposure to pilus-enriched fractions transiently increased cytosolic $Ca^{2+}$ levels in HBMEC, and this was found to be important for ASM surface display mediated by lysosomal exocytosis, as depletion of cytosolic $Ca^{2+}$ resulted in a significant decrease in ASM surface levels, ASM activity, and CRP formation.

**KEYWORDS** *Neisseria meningitidis*, acid sphingomyelinase, sphingolipids, superresolution microscopy, type IV pili

Acid sphingomyelinase (ASM) is a lipid hydrolase causing sphingomyelin breakdown and the release of ceramides, which associate into small ceramide-enriched membrane domains that fuse to larger ceramide-rich platforms (CRPs), thereby modulating membrane structures and signal transduction (1–3).

Several bacterial pathogens regulate ASM translocation and/or activity to exploit host sphingolipids during their infection processes (4–15). This is reflected by the importance of this enzyme in host defenses (mainly uptake and trafficking in phagocytes), as revealed for *Pseudomonas aeruginosa* (5) and for *Listeria monocytogenes* and *Neisseria gonorrhoeae* (7, 16, 17). In addition, ASM was also found to be crucial for bacterial uptake into nonphagocytic cells, including endothelial cells. In peripheral endothelial cells, *Staphylococcus aureus* infection increased ASM activity, and this contributed to the development of pulmonary edema (18). In brain endothelial cells,

**Citation** Peters S, Schlegel J, Becam J, Avota E, Sauer M, Schubert-Unkmeir A. 2019. *Neisseria meningitidis* type IV pili trigger $Ca^{2+}$-dependent lysosomal trafficking of the acid sphingomyelinase to enhance surface ceramide levels. Infect Immun 87:e00410-19. https://doi.org/10.1128/IAI.00410-19.

**Editor** Andreas J. Bäumler, University of California, Davis



Address correspondence to Alexandra Schubert-Unkmeir, aunkmeir@hygiene.uni-wuerzburg.de.

**Received** 23 May 2019
**Accepted** 24 May 2019
**Accepted manuscript posted online** 3 June 2019
**Published** 23 July 2019

ASM translocation and the increased activity caused by OpcA-expressing *Neisseria meningitidis* resulted in enhanced ceramide surface display, which was found to support bacterial uptake by recruitment of the ErbB2 receptor, involved in bacterial uptake into CRPs (6). This observation paralleled the finding obtained with the related species *N. gonorrhoeae* in phagocytic cells (16), where ASM caused the recruitment of CEACAM receptors in CRPs.

ASM localizes in lysosomes or in specialized lysosomal compartments named secretory lysosomes (19). Its activation may occur within this compartment by protein kinase Cδ-mediated phosphorylation (20, 21) or has been suggested to require translocation from the intracellular compartment to the extracellular leaflet of the cell membrane. For example, the application of hydrogen peroxide to mammalian cells induces a rapid $Ca^{2+}$-dependent ASM translocation by lysosomal exocytosis, followed by its activation (22), and plasmalemmal injury-triggered $Ca^{2+}$ influxes have been shown to induce the fusion of lysosomes with the plasma membrane, resulting in exocytosis and activation of ASM (23).

*N. meningitidis* (the meningococcus) is a human pathogen that colonizes the upper respiratory tract of approximately 10 to 40% of the healthy population (24, 25). In rare cases the pathogen can cause devastating invasive infections, resulting in sepsis and meningitis, predominantly in young infants and toddlers. Via its outer membrane protein OpcA, *N. meningitidis* is capable of triggering ASM translocation and increasing its activity as well as ceramide release and the formation of CRPs on the surface of brain endothelial cells (6). The ASM translocation elicited by OpcA critically relies on OpcA interaction with heparan sulfate proteoglycans and the subsequent activation of phosphatidylcholine-specific phospholipase C. In addition to OpcA, further meningococcal candidates are likely to contribute to ASM translocation, because infection-induced ASM translocation and ceramide surface display were reduced by only about 20 to 30% with an isogenic mutant lacking *opcA* (6).

As major adhesins, type IV pili (TfP) play key roles in pathogenic *Neisseria* species by mediating the contact with eukaryotic cell surfaces (26). The pilus fiber is composed of a single structural component, the major pilin, PilE. In addition to PilE, several other structural pilin proteins, including PilC, PilD, PilG, and PilF, and the minor pilins PilX, PilV, and ComP contribute to TfP function (27–31), which includes the uptake of DNA for natural transformation and bacterial movement (32, 33) and initiation of signal transduction cascades (34). Purified neisserial pili and pili from the bacterial crude membrane fraction have been shown to induce transient increases of cytosolic $Ca^{2+}$ levels in infected eukaryotic cells (35, 36). Moreover, pilus-induced $Ca^{2+}$ transients trigger lysosomal exocytosis, exposing lysosomal Lamp1 at the host cell surface (36).

In this study, we tested the hypothesis that the pilus-induced $Ca^{2+}$ flux in brain endothelial cells triggers lysosomal exocytosis, exposing ASM at the outer leaflet of the plasma membrane. We found that infection of human brain microvascular endothelial cells (HBMEC) with the highly piliated isolate *N. meningitidis* 8013 but not an isogenic pilus-deficient meningococcal mutant resulted in an increase in the amount of ceramide on the host cell surface in an amitriptyline-sensitive manner. Exposure of HBMEC to pilus-enriched fractions (PeF) also triggered transient ASM surface display, paralleled by increased surface Lamp1 levels. Importantly, inhibition of cytosolic $Ca^{2+}$ levels inhibited pilus-induced Lamp1 as well as ASM surface display and the formation of CRPs, indicating that ASM is delivered to the outer leaflet of the plasma membrane by pilus-induced lysosomal exocytosis.

## RESULTS

**Exposure of *N. meningitidis* strain 8013 to brain endothelial cells induces ceramide release and the formation of ceramide-enriched platforms.** We have recently shown that *N. meningitidis* strain MC58 causes a rapid but transient translocation of the acid sphingomyelinase (ASM) in human brain microvascular endothelial cells (HBMEC). In this system, OpcA interaction with heparan sulfate proteoglycans significantly contributed to ASM translocation and activity (6). The 80% residual cer-

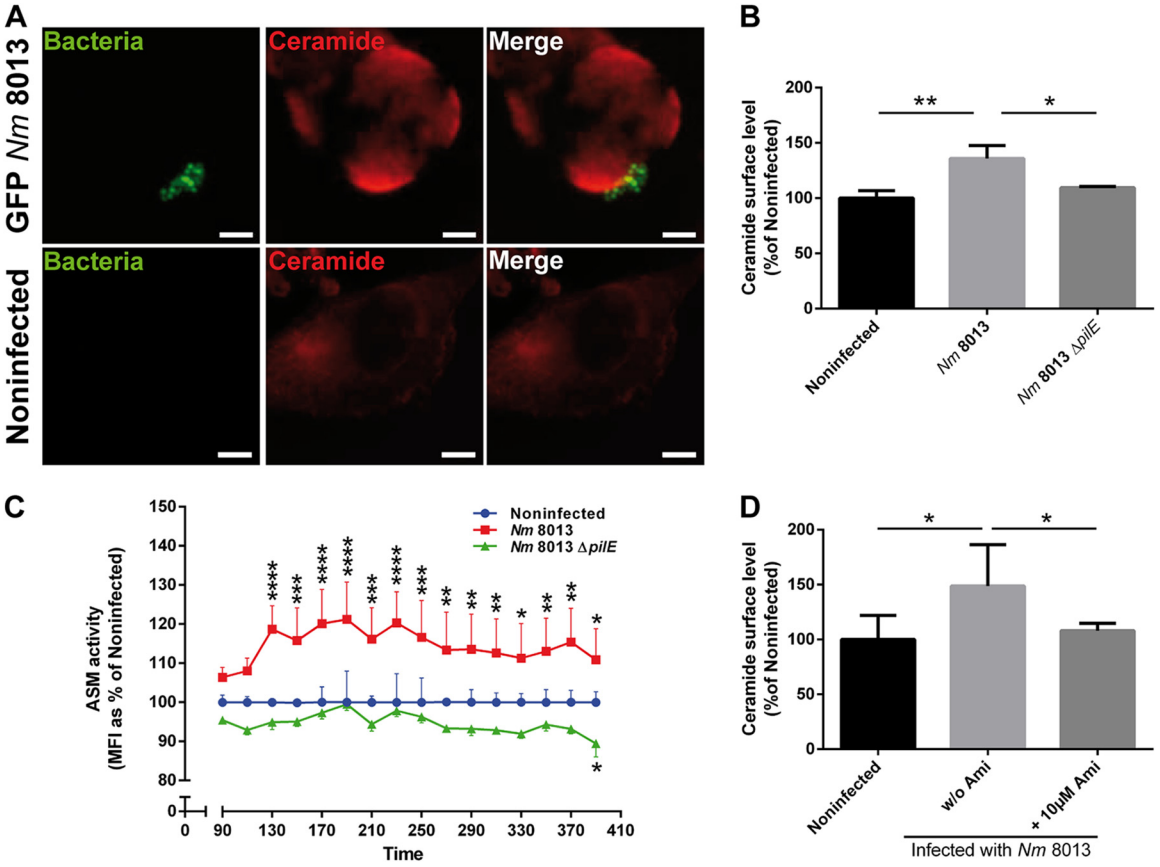


**FIG 1** Highly piliated *N. meningitidis* (*Nm*) strain 8013 activates ASM and the formation of CRPs on HBMEC. (A) HBMEC were grown to confluence in 8-well Ibidi $\mu$-slides and were infected with a GFP-expressing variant of *N. meningitidis* strain 8013 for 4 h or were left noninfected. Cells were washed, fixed in paraformaldehyde (FA), and stained with an anticeramide antibody and secondary Cy5-conjugated goat anti-mouse IgM (red). Images were captured using a Nikon Eclipse Ti-E inverted microscope with a 40× objective lens. Bars, 10 $\mu$m. (B) HBMEC were infected with wild-type strain *N. meningitidis* 8013 or an isogenic, pilus-deficient mutant (*N. meningitidis* 8013 Δ*pilE*) or were left noninfected for 4 h. Surface ceramide levels were determined by flow cytometry, and data are represented as the relative levels of ceramides on the host cell surface. Error bars represent the mean ± SD. One-way ANOVA with Dunnett's *post hoc* test was used to determine significance. *, $P < 0.05$; **, $P < 0.01$. (C) ASM activity was determined on HBMEC by measuring sphingomyelin hydrolysis to phosphorylcholine. Cells were seeded in black 96-well plates to confluence and infected with *N. meningitidis* 8013 or left noninfected (basal activity). Reported is the activity of ASM after infection with bacteria. Values show the mean ± SD from three independent experiments. MFI, mean fluorescence intensity. Two-way ANOVA was used to determine significance. *, $P < 0.05$; **, $P < 0.01$; ***, $P < 0.001$; ****, $P < 0.0001$. (D) HBMEC were infected with *N. meningitidis* 8013 for 4 h in the presence or absence of the ASM inhibitor amitriptyline (+10 $\mu$M Ami and w/o [without] Ami, respectively) or were left noninfected. Surface ceramide levels were determined by flow cytometry, and data are represented as the relative levels of ceramides on the host cell surface compared to that on noninfected cells. Values are expressed as a percentage of the level for noninfected cells ± SD. One-way ANOVA with Dunnett's *post hoc* test was used to determine significance. *, $P < 0.05$. All experiments were performed at least three times in duplicate.

amide induction by an isogenic *opcA*-deficient mutant suggested that other meningococcal components also contributed to ASM induction (6). To analyze whether the type IV pili (TfP) might be involved, a highly piliated, Opa-negative ($Opa^-$), *opcA*-deficient derivative of serogroup C, meningococcal strain 8013 (clone 12, also designated 2C4.3) (37), was applied and tested for its ability to contribute to ASM translocation in HBMEC. In common with *N. meningitidis* isolate MC58, immunofluorescence images demonstrate that a green fluorescent protein (GFP)-expressing variant of strain 8013 induced the formation of and adhered to CRPs (detected by the antibody 15B4) (Fig. 1A). HBMEC were then infected with *N. meningitidis* strain 8013 for 4 h, and surface ceramide levels on infected HBMEC were determined by flow cytometry (Fig. 1B; see also Fig. S1 in the supplemental material). *N. meningitidis* strain 8013 was found to be significantly effective at inducing ceramides on HBMEC (Fig. 1B), while this was not observed with a nonpiliated *pilE*-deficient mutant (*N. meningitidis* 8013 Δ*pilE*) (Fig. 1B). To analyze whether the surface ceramide release detected relied on ASM, we determined the

activity of the enzyme on living HBMEC after infection with the wild type and the *pilE*-deficient mutant. *N. meningitidis* strain 8013 but not the pilus-deficient mutant caused significant ASM activity, which peaked within 130 min postinfection (p.i.) (Fig. 1C). Corroborating the crucial role of ASM in *N. meningitidis* strain 8013-induced ceramide release, the latter was abrogated in HBMEC exposed to the ASM inhibitor amitriptyline 30 min prior to infection (Fig. 1D).

***N. meningitidis* recruits lysosomal ASM to the cell surface.** Because we detected ASM activity at the cell surface after *N. meningitidis* exposure, we reasoned that the enzyme should be translocated to and therefore be detectable at the outer leaflet of the plasma membrane. At 4 h following *N. meningitidis* treatment, ASM staining was observed in clusters on nonpermeabilized HBMEC close to bacterial microcolonies (Fig. 2A, left) suggesting its surface display. On a quantitative basis, this could be confirmed by flow cytometry (Fig. 2A, right). To test whether the translocation of ASM to the surface level of infected HBMEC might involve lysosomal exocytosis, Lamp1, a lysosomal marker, was detected on the surface of *N. meningitidis* 8013-infected HBMEC and analyzed by immunofluorescence microscopy and flow cytometry. The results revealed an increase in the level of Lamp1 membrane staining and Lamp1 surface levels as well as the codetection of both molecules, ASM and Lamp1, on infected HBMEC (Fig. 2B and C).

***N. meningitidis*-induced lysosomal exocytosis and ASM translocation to the plasma membrane are $Ca^{2+}$ dependent.** Lysosomal exocytosis requires $Ca^{2+}$ elevation for the fusion of predocked lysosomes with the plasma membrane. Because *N. meningitidis* induces $Ca^{2+}$ release from intracellular stores in infected human epithelial and endothelial cells (35, 38), we analyzed whether this would also apply to infection with *N. meningitidis* strain 8013 in our cell culture model system by using the calcium indicator Fluo-8. *N. meningitidis* strain 8013 significantly induced the cytosolic $Ca^{2+}$ concentration in infected cells compared to the uninfected controls (Fig. 3A and B and, for single cell analysis, Fig. 3C). To verify that the increase in calcium levels reflected the release from intracellular stores, $Ca^{2+}$ concentrations were again monitored by real-time immunofluorescence microscopy in cells treated with 50 $\mu$M 2-aminoethoxydiphenyl borate (2-APB), a chemical that acts to inhibit both inositol 1,4,5-trisphosphate receptors and transient receptor potential channels, prior to infection with meningococci. The inhibitor diminished calcium efflux in infected cells, supporting the finding that $Ca^{2+}$ was indeed released from the endoplasmic reticulum in HBMEC (Fig. 3A and B, right). If $Ca^{2+}$ mobilization is required for *N. meningitidis*-induced lysosomal exocytosis, 2-APB preexposure of HBMEC should affect the surface display of Lamp1, ASM, and ceramide as well as surface ASM activity. In fact, 2-APB dose dependently reduced the Lamp1 as well as ASM surface levels measured by flow cytometry (Fig. 4A and B). In addition, increased ASM activity and ceramide surface accumulation were not observed after 2-APB treatment (Fig. 4C and D), indicating that ASM translocation to the plasma membrane during meningococcal infection is mediated by $Ca^{2+}$-dependent lysosomal exocytosis.

***N. meningitidis* PilC1 is involved in ceramide release.** Two PilC alleles that encode two paralogous proteins, PilC1 and PilC2, have been described (27). PilC2 is expressed independently of PilC1 and mediates adhesion to some cell types, not including endothelial cells (27, 39), while the adhesive properties of TfP to endothelial cells depend on PilC1 (27). PilC1-deficient (PilC2 positive) mutants fail to adhere to endothelial cells, and moreover, PilC1-deficient mutants fail to trigger $Ca^{2+}$ release (35). To identify the role of PilC1 and PilC2 in ceramide release, we generated Δ*pilC1* and Δ*pilC2* mutant strains and analyzed their adhesive properties as well as ceramide accumulation on infected HBMEC by a gentamicin protection assay, immunofluorescence microscopy, and flow cytometry analysis. The Δ*pilC1* mutant showed much reduced adherence to HBMEC comparable to that of the nonpiliated Δ*pilE* mutant and was unable to increase ceramide levels or promote the formation of CRPs on infected cells, while these properties were fully retained in the Δ*pilC2* mutant (Fig. 5).

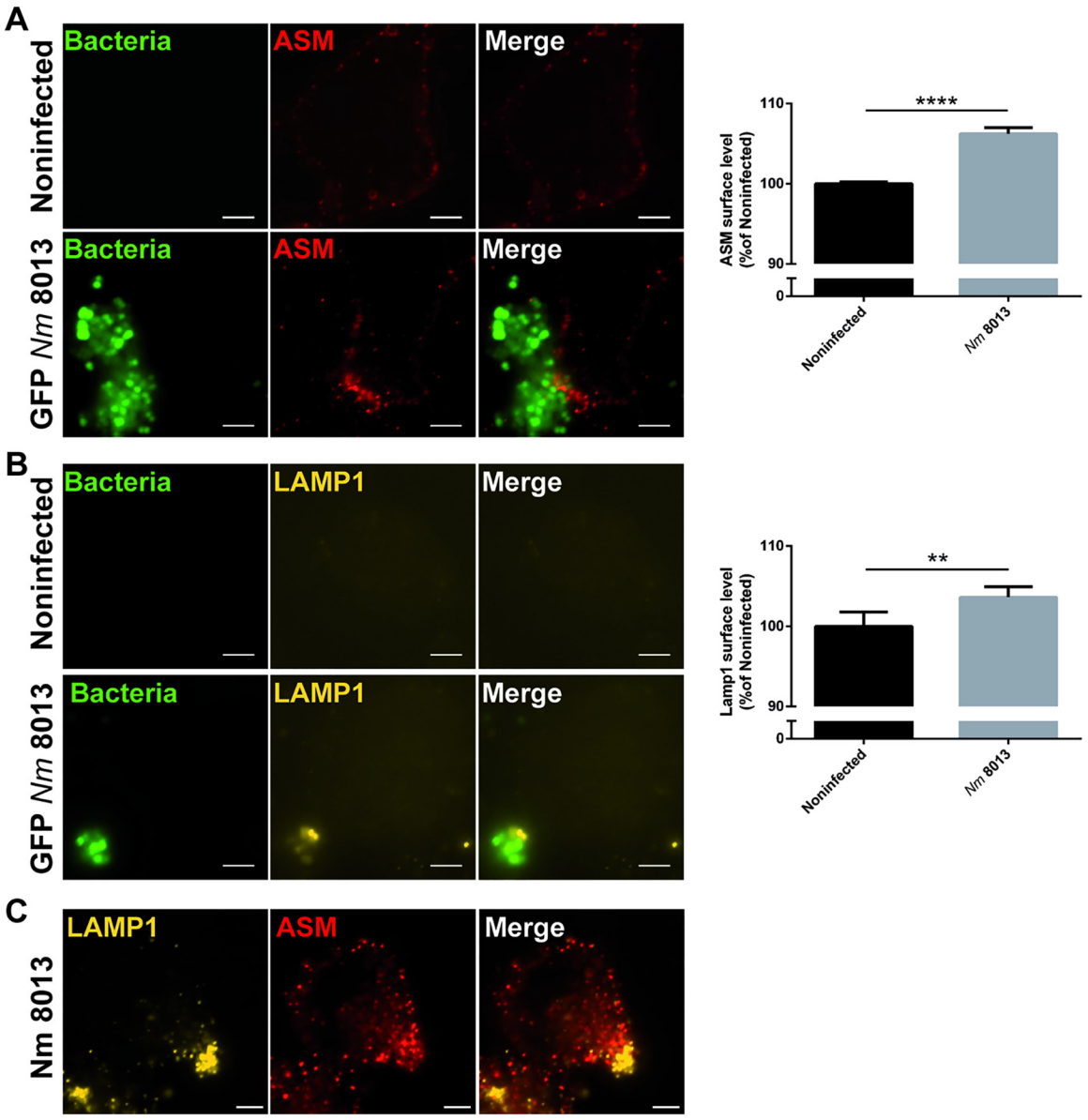


**FIG 2** *N. meningitidis* induces the translocation of lysosomal ASM and Lamp1 to the cell surface. HBMEC were grown to confluence in 8-well Ibidi $\mu$-slides and infected with the GFP-expressing *N. meningitidis* 8013 strain for 4 h or were left noninfected, and then ASM translocation as well as Lamp1 exposure on the host cell surface was evaluated. (A) (Left) Cells were washed, stained live on ice with a rabbit IgG anti-ASM antibody and secondary Cy5-conjugated anti-rabbit IgG F(ab′)$_2$, and then fixed in FA (red). Bars, 5 $\mu$m. (Right) ASM exposure on the plasma membrane was determined by flow cytometry of nonpermeabilized cells. Data show the mean ± SD from three independent experiments performed in duplicate. ****, $P < 0.0001$ by an unpaired, two-tailed Student's *t* test. (B) (Left) Cells were washed, stained live on ice with a mouse IgG PE-conjugated anti-Lamp1 antibody, and then fixed in FA (yellow). Bars, 5 $\mu$m. (Right) Lamp1 exposure to the plasma membrane was determined by flow cytometry of nonpermeabilized cells. Data show the mean ± SD from three independent experiments performed in duplicate. **, $P < 0.01$ by an unpaired, two-tailed Student's *t* test. (C) Cells were infected with the *N. meningitidis* 8013 strain for 4 h, washed, fixed in FA, and stained with a mouse IgG PE-conjugated anti-Lamp1 antibody (yellow), as well as rabbit IgG anti-ASM antibody and secondary Cy5-conjugated anti-rabbit IgG F(ab′)$_2$ (red). Bars, 5 $\mu$m.

**Depletion of $Ca^{2+}$ levels interferes with bacterial uptake.** We previously demonstrated that ASM translocation is of functional importance in meningococcal uptake (6). To corroborate the previous finding of the functional importance of ASM translocation in bacterial uptake, HBMEC were pretreated with 2-APB for 30 min prior to infection, and adhesion and invasion were determined. Indeed, the decrease in $Ca^{2+}$ levels caused by 2-APB affected *N. meningitidis* uptake by HBMEC (Fig. 6), which could also be observed after chelation of intracellular $Ca^{2+}$ by the acetoxymethyl ester of EGTA (EGTA-AM) (Fig. S2).

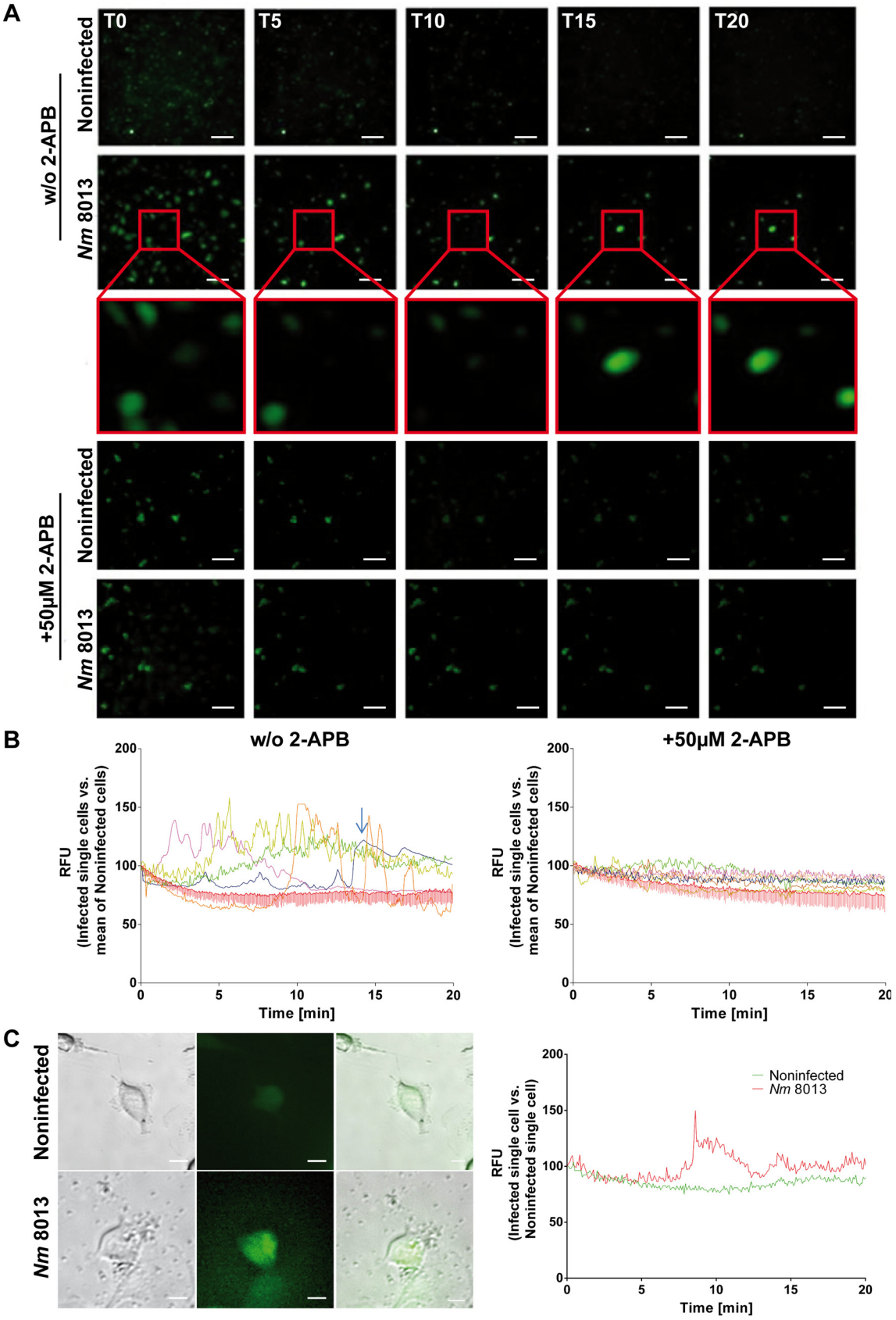


**FIG 3** *N. meningitidis* increases cytosolic $Ca^{2+}$ levels in brain endothelial cells derived from the endoplasmic reticulum. Fluo-8-loaded HBMEC were infected with *N. meningitidis* 8013 in the presence or absence of 50 $\mu$M 2-APB or were left noninfected, and cytosolic $Ca^{2+}$

(Continued on next page)

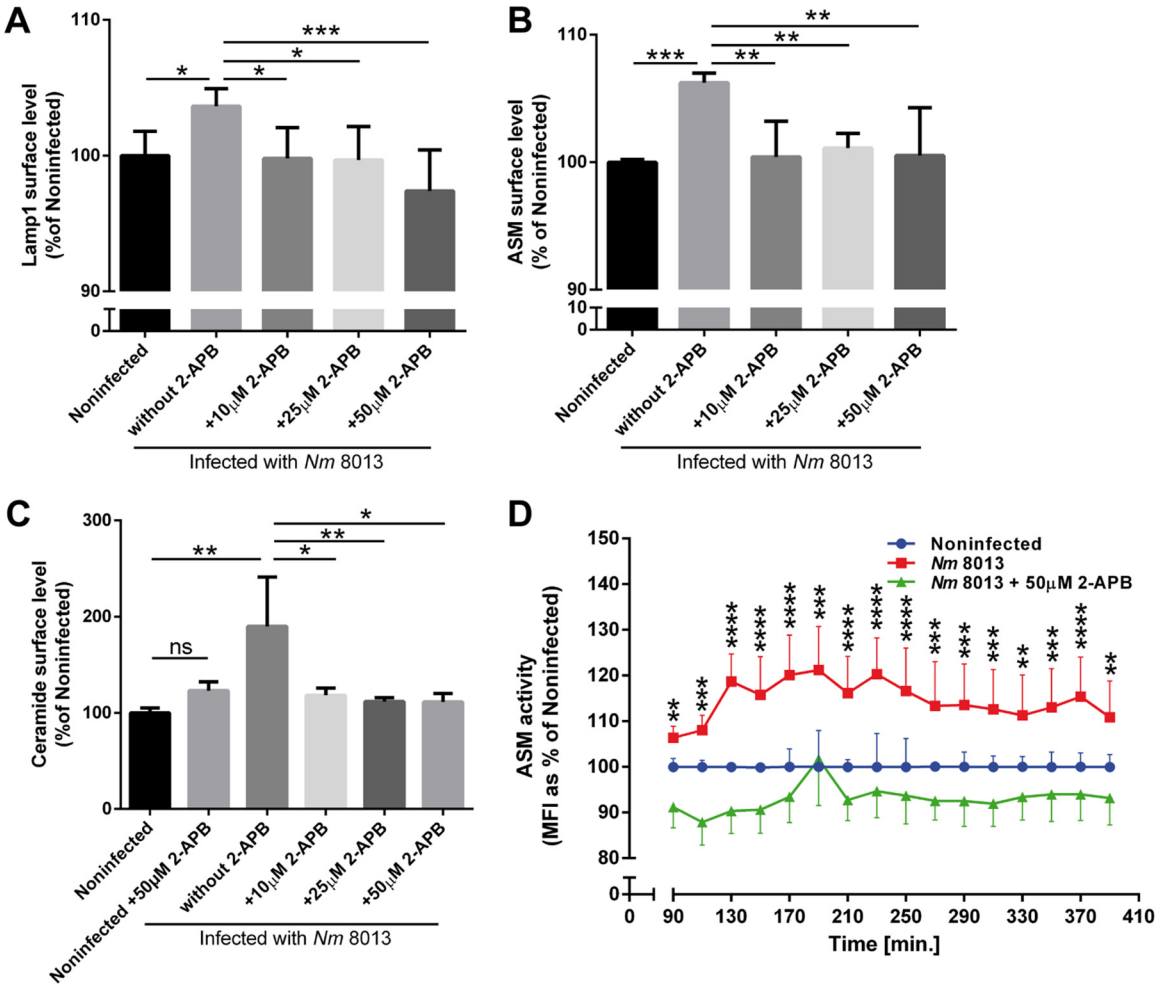


**FIG 4** *N. meningitidis*-induced ASM translocation to the plasma membrane is $Ca^{2+}$ dependent. HBMEC were treated with different concentrations of 2-APB (10, 25, 50 $\mu$M) for 30 min prior to infection with *N. meningitidis* 8013. *N. meningitidis*-induced Lamp1 exocytosis, ASM translocation, and ceramide surface levels were detected by flow cytometry analysis using a mouse IgG PE-conjugated anti-Lamp1 antibody (A), a mouse IgG2a anti-ASM antibody and secondary Cy3-conjugated anti-mouse IgG $F(ab')_2$ (B), or an anticeramide antibody and secondary Cy5-conjugated goat anti-mouse IgM (C). Data show the mean ± SD levels as a percentage of those for noninfected cells from three independent experiments performed in duplicate. One-way ANOVA with Dunnett's *post hoc* test was performed to determine significance. *, $P < 0.05$; **, $P < 0.01$; ***, $P < 0.001$. (D) ASM activity after infection with bacteria in the presence (50 $\mu$M) or absence of 2-ABP. Values show the mean ± SD from three independent experiments. Two-way ANOVA was used to determine significance. *, $P < 0.05$; **, $P < 0.01$; ***, $P < 0.001$; ****, $P < 0.0001$.

**Pilus-enriched fractions trigger calcium release and ASM translocation in HBMEC.** We next aimed at determining the role of pili as effectors in *N. meningitidis*-induced $Ca^{2+}$ release from HBMEC. Pilus-enriched fractions purified from the piliated wild-type meningococcal strain 8013 did not contain detectable levels of porins (a major pathogenicity factor involved in $Ca^{2+}$ influx into the host cell [44]), while the presence of pilin in the preparations was visualized with a monoclonal antibody raised against PilE (Fig. S3). Cytosolic $Ca^{2+}$ concentrations were determined in HBMEC loaded

**FIG 3** Legend (Continued)
concentrations were monitored over 20 min. Images were captured using a Nikon Eclipse Ti-E inverted microscope and analyzed using NIS Elements AR software (Nikon). (A) Representative fluorescence images taken at the indicated time points (0, 5, 10, 15, and 20 min [T0, T5, T10, T15, and T20, respectively]) are shown. Images were taken at a ×20 magnification. Bars, 100 $\mu$m. (B) Fluorescence data from representative cells were exported and are shown as the number of relative fluorescence units (RFU) relative to the start fluorescence intensity value. Images show the results for infected single cells (left) or 2-APB-treated cells (right) versus the mean for noninfected cells. The arrow indicates the results for a single cell which appears at 15 min in the inset in panel A. 2-APB, 2-aminoethoxydiphenyl borate. (C) Representative single-cell analysis results. Pictures (left) show single cells which were analyzed for their fluorescence intensity (right). Bars, 10 $\mu$m.

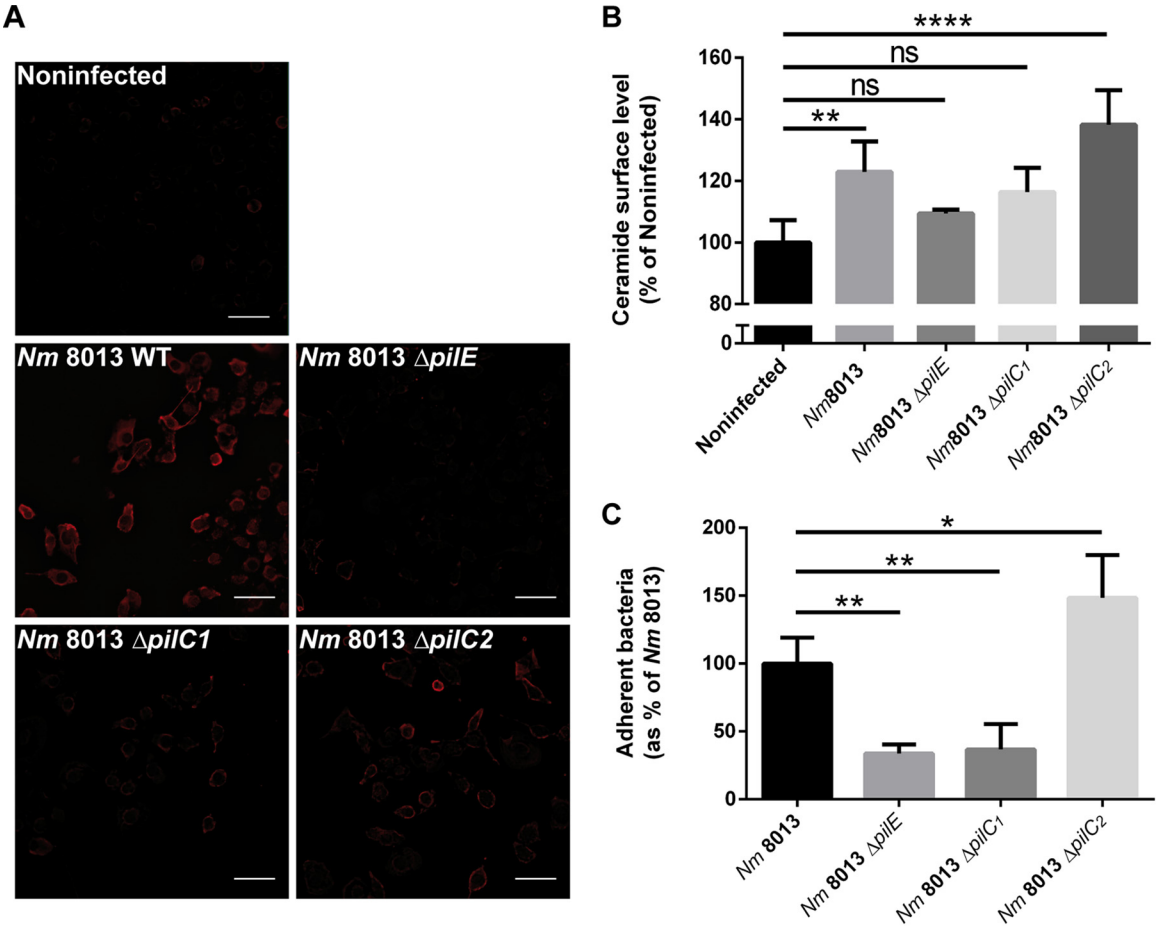


**FIG 5** Ceramide release and CRP formation in response to isogenic Δ*pilC1* or Δ*pilC2* meningococcal mutants. (A) HBMEC were grown to confluence in 8-well Ibidi $\mu$-slides and were infected with wild-type (WT) strain *N. meningitidis* 8013 or isogenic meningococcal mutant *N. meningitidis* 8013 Δ*pilE*, *N. meningitidis* 8013 Δ*pilC1*, or *N. meningitidis* 8013 Δ*pilC2* for 4 h or were left noninfected. Cells were washed, fixed in FA, and stained with an anticeramide antibody and secondary Cy5-conjugated goat anti-mouse IgM (red). Images were captured using a Nikon Eclipse Ti-E inverted microscope with a 20× objective lens. Bars, 100 $\mu$m. The results of one of three reproducible experiments are shown. (B) HBMEC were infected with wild-type strain *N. meningitidis* 8013 or isogenic mutant *N. meningitidis* 8013 Δ*pilE*, *N. meningitidis* 8013 Δ*pilC1*, or *N. meningitidis* 8013 Δ*pilC2* or were left noninfected for 4 h. Surface ceramide levels were determined by flow cytometry, and data are represented as the relative levels of ceramides on the host cell surface. (C) HBMEC were infected with the *N. meningitidis* 8013 wild-type strain or the indicated mutants (the Δ*pilE*, Δ*pilC1*, or Δ*pilC2* mutant) for 4 h at an MOI of 100. Adhesion was determined by a gentamicin protection assay. Error bars represent the mean ± SD. One-way ANOVA with Dunnett's *post hoc* test was used to determine significance. *, $P < 0.05$; **, $P < 0.01$; ****, $P < 0.0001$; ns, not significant.

with the fluorescent $Ca^{2+}$ indicator Fluo-8 and treated with 2.5 $\mu$g/ml of pilus-enriched fractions. Immediately after addition, pilus-enriched fractions (but not control buffer [not shown]) induced a significant cytosolic $Ca^{2+}$ increase within 2 to 5 min, and the levels quickly returned to the baseline levels (Fig. 7A). Lysosomal exocytosis was next monitored in LysoTracker-loaded cells exposed to 2.5 $\mu$g/ml of pilus-enriched fractions or medium alone (in the absence of $Ca^{2+}$). A rapid decrease in the fluorescence signal was observed after treatment with pilus-enriched fractions, indicating that fusion of the lysosomal membrane with the plasma membrane and LysoTracker release occurred (Fig. 7B, pilus-enriched fractions [PeF]). Treatment of HBMEC with 2.5 $\mu$g/ml of the pilus-enriched fractions slightly but significantly increased both ASM and ceramide plasma membrane surface display, as determined by flow cytometry at 2 h after exposure (Fig. 7C). In addition, the pilus-enriched fraction induced 2-APB-sensitive ASM surface activity (Fig. 7E).

The pilus-enriched fraction also efficiently induced CRP formation on HBMEC. This was first revealed by standard microscopy (Fig. 7D), and thereafter, the distribution of CRPs was analyzed by single-molecule sensitive superresolution microscopy using

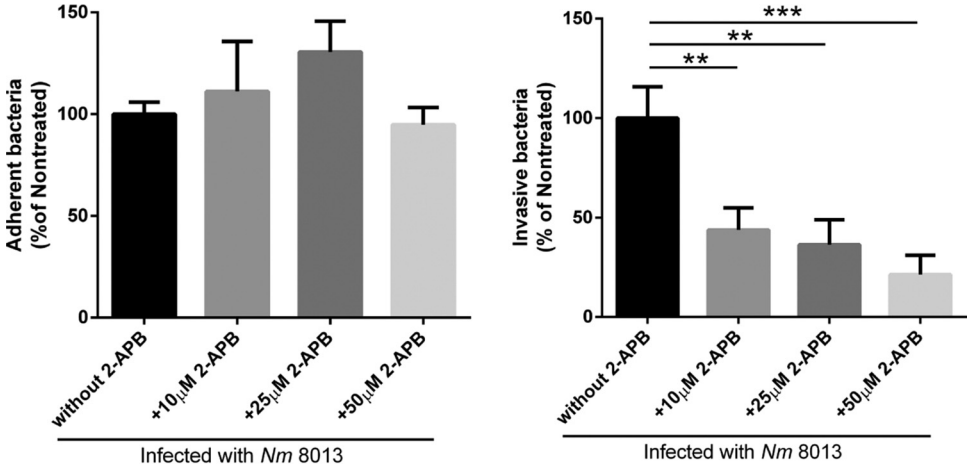


**FIG 6** Depletion of the $Ca^{2+}$ level interferes with invasion of *N. meningitidis* strain 8013 into HBMEC. HBMEC were pretreated with different concentrations (10, 25, 50 $\mu$M) of the 1,4,5-trisphosphate receptor inhibitor 2-APB. Afterwards, cells were infected for 4 h at an MOI of 100, and adhesion (left) and invasion (right) were determined by a gentamicin protection assay. All results show the mean $\pm$ SD levels as a percentage of the levels for untreated control cells from three independent experiments performed in duplicate. *P* values are relative to the values for untreated control cells and were determined by an ordinary one-way ANOVA with Dunnett's *post hoc* test. **, $P < 0.01$, ***, $P < 0.001$.

indirect immunocytochemistry and direct stochastic optical reconstruction microscopy (*d*STORM) (40, 41) (Fig. 8). The overall number of CRPs with a size of ~80 nm (41) in the plasma membrane was significantly increased in HBMEC after 2 h of exposure to the pilus-enriched fractions, and the formation of CRPs could be prevented by treatment with 2-APB (Fig. 8A to D).

## DISCUSSION

ASM has been shown to be an important factor in pathogen infection and survival. Some bacterial pathogens can target ASM and thereby modulate microdomain reorganization, which can alter cellular internalization or cell death (5–8, 11, 16–18, 43). As a prerequisite, lysosomal ASM has to be relocalized at the cell surface and activated; however, the precise mechanism by which this is achieved during bacterial infections remains unknown. In this study, we tested the hypothesis that the meningococcal pilus-induced increase in cytosolic $Ca^{2+}$ triggers lysosomal exocytosis and increases the amount of cell surface ASM, followed by lipid microdomain formation. We demonstrate that the highly piliated *N. meningitidis* isolate 8013 but not an isogenic pilus-deficient mutant was effective at inducing ceramides on HBMEC. Increased ceramide surface levels reflected increased ASM activity and were abrogated in the presence of the ASM inhibitor amitriptyline. We showed that pilus-enriched fractions also triggered the transient translocation of ASM to the host cell surface. We provided microscopic evidence that live, piliated bacteria as well as pilus-enriched fractions induced transient increases in cytosolic $Ca^{2+}$ levels in HBMEC and triggered lysosomal exocytosis, as detected by exposure of Lamp1. Of importance, we finally showed that depletion of cytosolic $Ca^{2+}$ transients with 2-APB, a chemical that acts to inhibit inositol 1,4,5-trisphosphate receptors, abolished not only Lamp1 levels but also ASM translocation and, thus, the formation of CRPs on *N. meningitidis*-infected HBMEC or cells treated with pilus-enriched fractions.

We have recently shown that *N. meningitidis* strains can transiently translocate ASM if they express the OpcA protein and use CRPs as a port of entry into HBMEC (6). However, further meningococcal factors besides OpcA are likely to contribute to ASM translocation and the generation of ceramides, since infection of brain endothelial cells with an isogenic mutant lacking *opcA* resulted in a decrease in the amount of ceramide on the host cell surface of only about 20 to 30% (6). TfP of pathogenic *Neisseria* are essential during the initial stage of infection and are known to initiate a signal

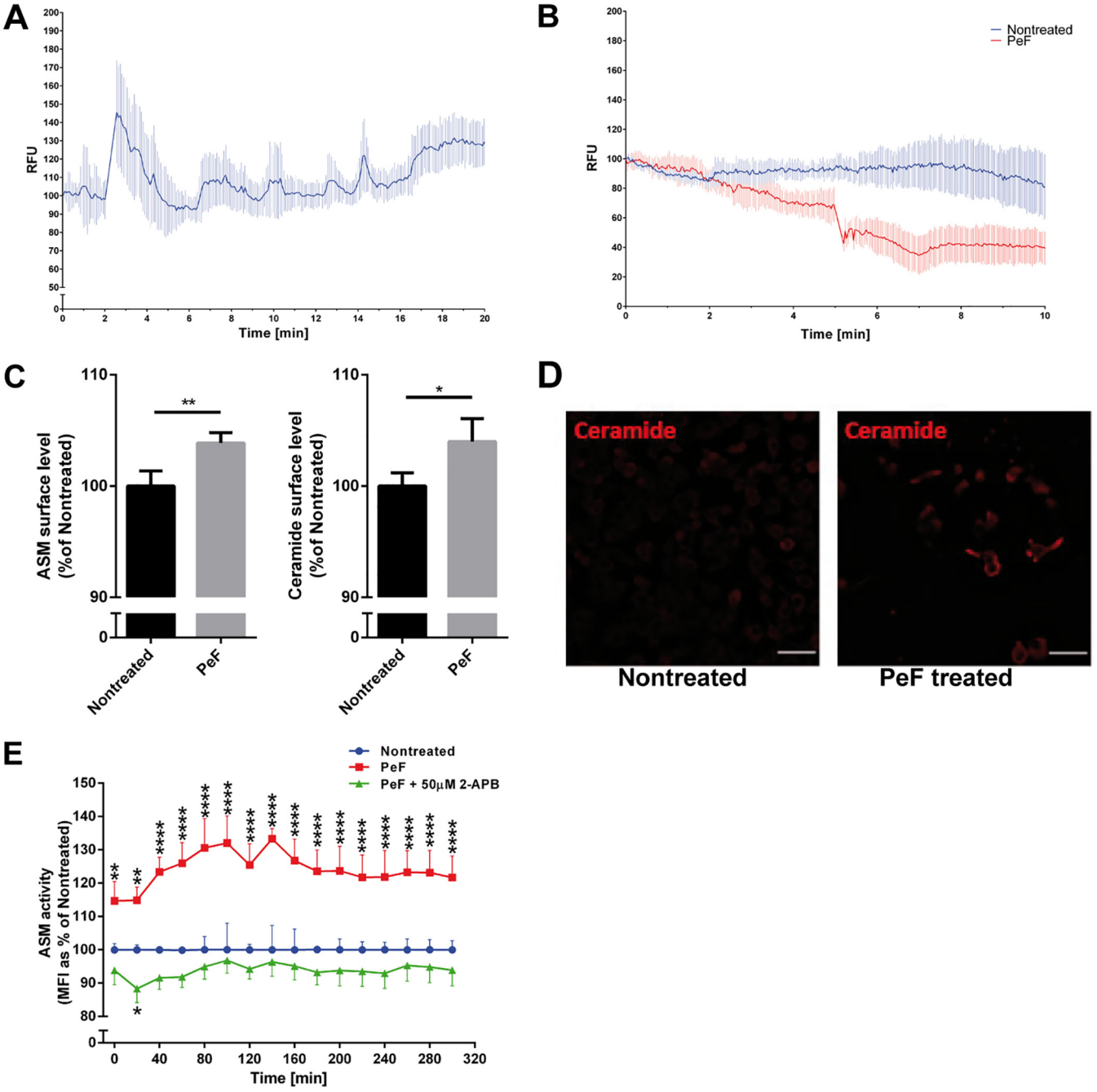


**FIG 7** Effect of pilus-enriched fractions on $Ca^{2+}$ fluxes, ASM translocation and activity, and ceramide release. (A) HBMEC were loaded with Fluo-8 and treated with 2.5 $\mu$g pilus-enriched fraction (PeF) from *N. meningitidis* 8013 in $Ca^{2+}$-free medium. Cytosolic $Ca^{2+}$ concentrations were monitored over 10 min using a Nikon Eclipse Ti-E inverted microscope and analyzed using NIS Elements AR software (Nikon). Fluorescence data from representative cells were exported and are shown as the mean ± SD number of relative fluorescence units relative to the starting fluorescence intensity value. (B) HBMEC were loaded with LysoTracker green (80 nM) and treated with PeF (2.5 $\mu$g) in $Ca^{2+}$-free medium. Fluorescence signals were monitored over 10 min. Fluorescence data from representative cells were exported and are shown as the mean ± SD number of relative fluorescence units relative to the starting fluorescence intensity value. Note the disappearance of the LysoTracker green signal after addition of PeF, indicative of lysosomal exocytosis. (C) Cells were maintained in infection medium and incubated with PeF (2.5 $\mu$g) from *N. meningitidis* 8013. The pilus-induced translocation of ASM and ceramide surface levels were detected by flow cytometry analysis. Data show the mean ± SD from three independent experiments performed in duplicate. *P* values were determined by an unpaired, two-tailed Student's *t* test. *, $P < 0.05$; **, $P < 0.01$. (D) Cells were grown to confluence in Ibidi $\mu$-slides and were incubated with PeF (2.5 $\mu$g) from *N. meningitidis* 8013 or were left nontreated. Cells were washed, fixed in FA, and stained with an anticeramide antibody and secondary Cy5-conjugated goat anti-mouse IgM (red). Bars, 10 $\mu$m. (E) Cells were incubated with PeF or left nontreated, and ASM activity was determined. Reported is the activity of ASM after incubation of the cells with PeF (1 $\mu$g) from *N. meningitidis* 8013. Values show the mean ± SD from three independent experiments. A two-way ANOVA was used to determine significance. *, $P < 0.05$; **, $P < 0.01$; ****, $P < 0.0001$.

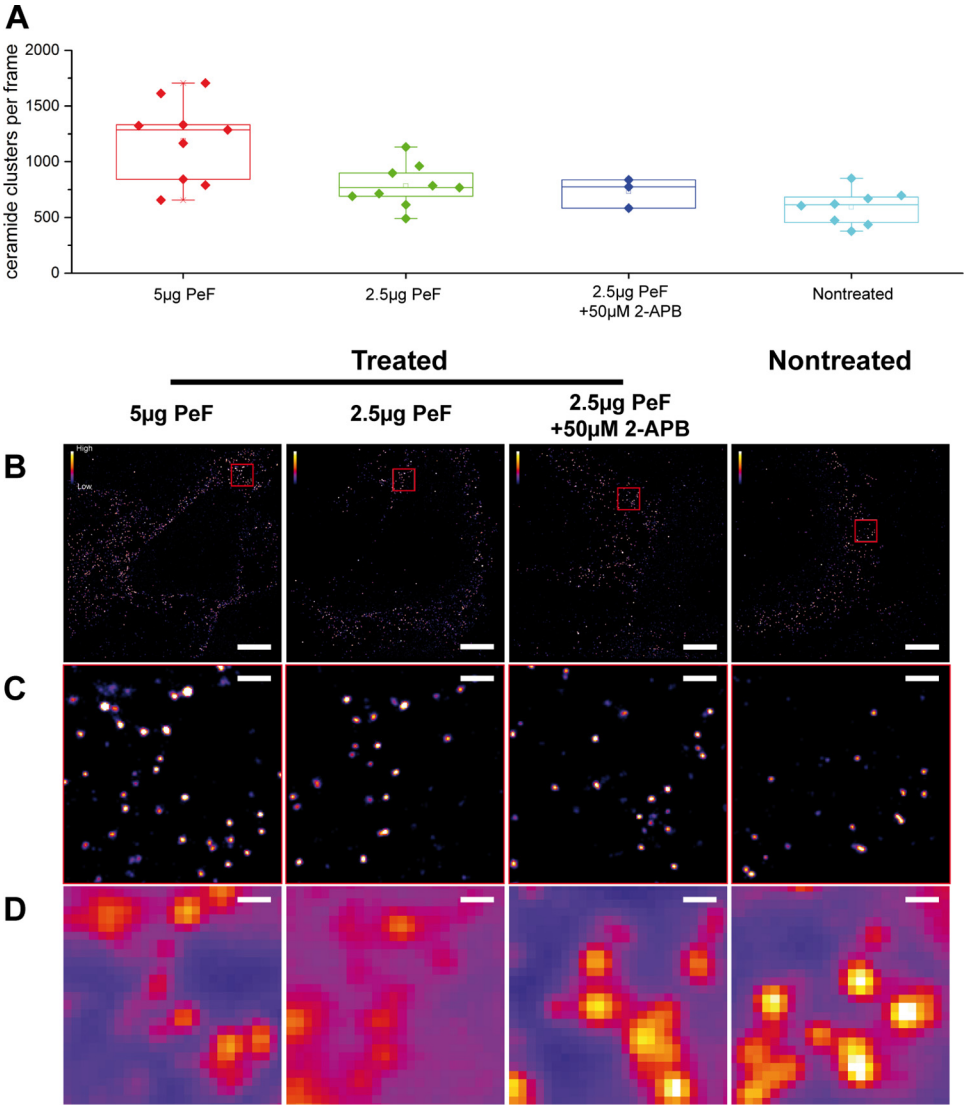


**FIG 8** Treatment of HBMEC with pilus-enriched fractions increases the number of plasma membrane-associated CRPs. (A) Quantification of subdiffraction-sized CRPs within the plasma membrane of HBMEC pretreated with different concentrations of the pilus-enriched fraction (PeF) at 5 $\mu$g, 2.5 $\mu$g, or 2.5 $\mu$g or with 50 $\mu$M 2-APB or not treated. The superresolution images show a dose-dependent enrichment of sphingolipid nanodomains upon pilus treatment. (B) Representative *d*STORM images of HBMEC treated with the indicated concentrations of PeF (as shown in panel A). (C) Images of the corresponding *d*STORM insets (red squares) from panel B, illustrating the increase in the number of CRPs induced by the addition of PeF. (D) Conventional diffraction-limited microscopy of the sections shown in panel C. Bars, 5 $\mu$m (B) and 500 nm (C and D).

transduction cascade, resulting in tyrosine phosphorylation of cytoskeletal proteins (34). In addition, they induce $Ca^{2+}$ transients in cultures of epithelial cells and monocytes (35, 36, 44). Here, we used real-time fluorescence imaging to examine $Ca^{2+}$ levels in HBMEC during infection with piliated bacteria. Like the purified proteins and as shown for A431 and ME180 cells, live bacteria also triggered changes in cytosolic $Ca^{2+}$ fluxes (35, 36). Besides TfP, the pilus-associated *Neisseria* porins also trigger a transient rise in cytosolic $Ca^{2+}$ levels. In contrast to TfP-induced $Ca^{2+}$ increases, the porin-triggered $Ca^{2+}$ influx is rapid, occurs within 2 min after exposure of the protein, and stimulates endosome exocytosis (45, 46). Pilus-associated porins are supposed to insert into the host membrane to trigger an influx of $Ca^{2+}$ ions from the external environment (44). In our experimental setting, we can exclude the possibility of any effects related to *N. meningitidis* porins, since experiments were performed in $Ca^{2+}$-free medium and we could not detect any porin proteins on our pilus-enriched fraction preparation.

$Ca^{2+}$ transients in cultures of epithelial cells have been thought to be transduced by the proposed pilus receptor, CD46 (35), as it could be blocked by anti-CD46 antibodies (35). However, recent publications have highlighted the specific interaction between the meningococcal ligands PilE and PilV and the cellular host receptor CD147 to be essential for meningococcal adhesion to human brain endothelial cells and colonization of human blood vessels (42). Whether $Ca^{2+}$ transients might be transduced by CD147 needs further investigations.

$Ca^{2+}$ is a highly versatile intracellular signal that can regulate many different cellular functions (49, 50), and the effects of $Ca^{2+}$ fluxes in response to *N. meningitidis* are likely to be various. These transients have, for example, been demonstrated to increase the intracellular survival of the related species *N. gonorrhoeae*. $Ca^{2+}$-dependent lysosomal exocytosis leads to the redistribution of Lamp1 to the plasma membrane and the release of the luminal content of the vesicle to the extracellular milieu. Lamp1 cleavage at the host cell surface by the secreted neisserial IgA protease finally results in lysosome remodeling and enhanced bacterial survival within cells (36, 45, 51). The data presented in this study now show that the exocytic events resulting from the pilus-induced $Ca^{2+}$ transients also bring ASM to the outer leaflet of the plasma membrane. However, further studies are required to determine the exact mechanism of ASM enzyme activation in response to TfP.

In nonsecretory cells, most lysosomes that undergo $Ca^{2+}$-regulated exocytosis belong to a peripheral population (52). By this means, calcium is primarily responsible for the fusion rather than the recruitment of lysosomes to the plasma membrane (52). Peripheral lysosomes were subsequently identified to be the major population of intracellular vesicles that respond to $Ca^{2+}$ fluxes by fusing with the plasma membrane and promoting plasma membrane repair (23, 52–54). Restoring membrane integrity is crucial to preclude necrosis and apoptosis and reduce inflammation from necrotic cells. Interestingly, host cell entry by *Trypanosoma cruzi* mimics a process of plasma membrane injury and repair that involves $Ca^{2+}$-mediated exocytosis of lysosomes and the delivery of ASM to the outer leaflet of the plasma membrane, followed by a rapid form of endocytosis that internalizes membrane lesions (53, 55). A similar mechanism was recently observed during the entry of adenovirus into nonphagocytic cells (56). The viral membrane lytic protein protein VI induces small plasma membrane lesions and stimulates $Ca^{2+}$ influx and lysosomal exocytosis, finally resulting in the release of ASM and the degradation of sphingomyelin to ceramide lipids in the plasma membrane (56). In contrast to the stimulation of lysosomal exocytosis by *T. cruzi* or adenovirus infection, the *N. meningitidis*-mediated increase of $Ca^{2+}$ transients did not involve small plasma membrane lesions or $Ca^{2+}$ influx from the extracellular milieu; instead, $Ca^{2+}$ transients arose from the endoplasmic reticulum.

Besides bacterial or viral infection, ASM is exposed to the host cell surface in response to further stimuli, including CD95 or DR5 ligation, UV irradiation, or membrane damage (5, 57–61). Recently, the application of the reactive oxygen species (ROS) hydrogen peroxide to mammalian cells has been demonstrated to induce a rapid $Ca^{2+}$-dependent ASM translocation by lysosomal exocytosis (22). In contrast, CD95 or DR5 activation induces ROS-dependent ASM trafficking independently of $Ca^{2+}$ (58). The precise mechanism for $Ca^{2+}$-independent ASM externalization is not well understood and might involve protein kinase C$\delta$ phosphorylation of ASM and translocation to the plasma membrane (20). Taken together, in this study, we provide experimental evidence supporting the conclusion that ASM, which resides within lysosomes, can be exocytosed from *N. meningitidis*-infected brain endothelial cells in a $Ca^{2+}$-dependent manner and act on the outer plasma membrane to promote the formation of CRPs.

## MATERIALS AND METHODS

**Bacterial strains.** *N. meningitidis* strain 8013 (clone 12, also designated 2C4.3) is a piliated capsulated Opa- and Opc-negative variant of the serogroup C meningococcal clinical isolate 8013 (sequence type 77 [ST77]/ST8 clonal complex [CC]; Institut Pasteur, 1989) and was kindly provided by M. Taha (37). The characteristics of the wild-type strain and the mutants are summarized in Table S1 in the supplemental material. Bacteria were grown overnight on Columbia blood agar plates (bioMérieux) at 37°C in 5% $CO_2$

and cultured on the next day in PPM+ medium (proteose-peptone medium supplemented with 1× Kellogg´s supplement, 0.01 M $MgCl_2$, and 0.005 M $NaHCO_3$). Pilus mutants were grown overnight on GC agar plates (37°C, 5% $CO_2$) with spectinomycin (75 $\mu$g/ml) and were cultured in the same medium used for the wild type but supplemented with additional spectinomycin (75 $\mu$g/ml).

**Cell culture.** Immortalized human brain microvascular endothelial cells (HBMEC) were kindly provided by K. S. Kim (62) and were cultured as described previously (63). Briefly, cells were cultured in RPMI 1640 medium supplemented with 1% sodium pyruvate (1 mM), 1% L-glutamine (2 mM), and 1% nonessential amino acids (all purchased from GE Healthcare, Little Chalfont, UK) plus 5 U/ml heparin (Biochrom, Berlin, Germany) and 30 $\mu$g/ml endothelial cell growth supplement (ECGS; CellSystems, Troisdorf, Germany). Cells were incubated at 37°C in 5% $CO_2$ in a humidified atmosphere.

**Infection assays.** Adhesion and invasion were determined by using gentamicin protection assays. Cells at between the 10th and 25th passages were used for infection assays at a density of $4 \times 10^5$ cells/well, with bacteria used at a multiplicity of infection (MOI) of 100, unless indicated otherwise, as described previously (6).

**Reagents and antibodies.** The following antibodies were used in this study: mouse IgG2a anti-ASM (clone ab74281; Abcam), rabbit IgG anti-ASM (clone H181; Santa Cruz), mouse IgM anticeramide (clone MID 15B4; Enzo Life Science), rabbit IgG anticeramide (kindly provided by E. Bieberich [41]), mouse IgG phycoerythrin (PE)-conjugated anti-Lamp1 (clone H4A3; Santa Cruz), mouse IgG anti-PilE (SM1; M. Virji [66]), polyclonal rabbit anti-PorB (Genosys Biotechnologies), a mouse IgM isotype control (clone ICIGMPU; Immunostep), a mouse IgG1 isotype control (clone PPV-06; Invitrogen), and a normal rabbit IgG isotype control (clone sc-2027; Santa Cruz). The following secondary conjugated antibodies, all of which were purchased from Jackson ImmunoResearch, were used in this study: Cy5-conjugated goat anti-mouse IgM, Cy5-conjugated goat anti-rabbit IgG (H+L), Cy3-conjugated goat anti-rabbit IgG (H+L), Cy3-conjugated rabbit anti-mouse IgG $F(ab')_2$, and peroxidase-conjugated goat anti-mouse IgG and IgM (H+L). The isotype and secondary antibody controls are shown in Fig. S4. The following reagents were used in this study: 2-aminoethoxydiphenyl borate (2-APB; Tocris Bioscience) was used at a final concentration of 10, 25, or 50 $\mu$M and did not affect bacterial growth or fitness when applied under infection conditions. Hoechst 33342 (Invitrogen) was used for nuclear staining at a final concentration of 1 $\mu$g/ml, the calcium indicator dye Fluo-8 (Abcam) was used at a final concentration of 4 $\mu$M, and LysoTracker green DND-26 (Invitrogen) was used at a concentration of 80 nM. All compounds were dissolved in dimethyl sulfoxide (DMSO), and the final concentration of DMSO in the culture wells never exceeded 0.1%.

**Flow cytometry.** At 3 days prior to the experiment, $1.25 \times 10^5$ cells/ml were seeded in a 24-well plate and were grown to approximately $1 \times 10^6$ cells/ml. On the day of the infection experiment, cell medium was replaced by RPMI 1640 medium plus 10% human serum and, if indicated, preincubated for 30 min with different concentrations of 2-APB. Cells were infected with the bacteria for 4 h. After infection, the cells were washed once with phosphate-buffered saline (PBS), trypsinized, and harvested in an Eppendorf tube. After washing with ice-cold fluorescence-activated cell sorting (FACS) buffer (5% fetal calf serum [FCS] in PBS), the cells were incubated with either mouse IgM anticeramide (1:30 in FACS buffer), mouse IgG PE-conjugated anti-Lamp1 (1:20 in FACS buffer), mouse IgG2a anti-ASM (1:250 in FACS buffer), or the corresponding isotype control antibodies (1:100 in FACS buffer) for 1.5 h at 4°C in the dark. After incubation, the cells were washed three times with FACS buffer and incubated with the appropriate secondary antibodies (1:500 in FACS buffer) for 30 min. Then, the cells were washed three times with FACS buffer and were fixed in 3.7% paraformaldehyde (FA; in PBS) for 30 min at 4°C. Afterwards, the cells were washed 3 times with FACS buffer and 500 $\mu$l was transferred into a FACS tube for measurement. Ten thousand cells were analyzed using a FACSCalibur flow cytometer (BD Bioscience), and the data were analyzed and graphed using FlowJo (v10) software (FlowJo, LLC).

**ASM activity assay.** For determination of ASM surface activity, a commercially available acid sphingomyelinase activity assay kit from Echelon was used with some adaptations to the manufacturer's protocol. One day prior to the infection experiment, $0.75 \times 10^4$ cells were seeded into a black-walled, black-bottom 96-well plate (Thermo Scientific). On the day of infection, the growth medium was replaced with RPMI 1640 medium plus 10% human serum, and infection assays were carried out for 2 h at 37°C in 5% $CO_2$. When indicated, cells were pretreated with 50 $\mu$M 2-APB for 30 min prior to infection. After infection, cells were washed once with PBS and the ASM substrate was added directly to the cells. For pilus-treated samples, 1 $\mu$g of the preparation was added to the cells right after the substrate was added. The activity of ASM was then detected in a spectrophotometer (Infinite F200 Pro Reader; Tecan Group, Maennedorf, Switzerland) at a 360-nm excitation wavelength and a 460-nm emission wavelength every 20 min for 5 h.

**Immunofluorescence microscopy.** For ceramide staining, $2.5 \times 10^4$ cells/well were seeded in 8-well chamber $\mu$-slides (Ibidi) and grown overnight. Cells were infected with bacteria for 4 h, washed with PBS, and fixed for 20 min with 3.7% paraformaldehyde. For the indicated experiments, cells were infected with GFP-expressing *N. meningitidis* strain 8013, a derivative of *N. meningitidis* 8013 expressing GFP from the plasmid pEG2-Ery (64). After fixation, cells were washed two times with PBS and blocked for 5 min in blocking buffer (1% FCS, 2% bovine serum albumin [BSA] in PBS). Then, the cells were washed and incubated with the primary antibody (1:200 dilution in blocking buffer) for 45 min at room temperature (RT), followed by treatment with the appropriate Cy fluorescent dye-labeled secondary antibody (1:200 in blocking buffer) for 45 min. (For ASM and LAMP1, cells were stained live on ice before fixation.) The samples were covered with PBS, and images were taken using a Nikon Eclipse Ti-E inverted microscope equipped with an Okolab incubator set to 37°C. Images were taken at a ×40 magnification and processed and analyzed using ImageJ software.

**LSM and *d*STORM.** Laser scanning microscopy (LSM) and *d*STORM imaging were performed as previously described (42). Briefly, HBMEC were seeded into 0.2% gelatin-coated 8-well plates on coverslip II slides (Sarstedt) at a concentration of $3 \times 10^4$ cells per well. After 24 h, the cells were treated with the amounts of pilus-enriched fractions indicated above for 2 h. After washing, the cells were labeled on ice with ~2-$\mu$g/ml rabbit anti-C16/24 ceramide IgG antibody for 50 min in cell culture medium and again washed. The cells were then fixed with 3% formaldehyde and 0.3% glutaraldehyde for 15 min on ice and 30 min at RT. After washing and blocking for 30 min with 5% BSA in PBS, staining with a secondary Alexa Fluor 647-conjugated goat anti-rabbit $F(ab')_2$ IgG fragment followed by 1 h in 5% BSA blocking buffer was performed. Cells were washed and again fixed with 2% formaldehyde and 0.2% glutaraldehyde to immobilize the antibodies. *d*STORM imaging was performed in switching buffer, consisting of 100 mM $\beta$-mercaptoethylamine (MEA; Sigma) in PBS, adjusted to pH 7.4. An inverted wide-field fluorescence microscope (model IX-71; Olympus) equipped with an oil-immersion objective (60×; numerical aperture, 1.45; Olympus) was used for superresolution measurements. Alexa Fluor 647 fluorophores were excited with a 641-nm diode laser (model Cube 640-100C; Coherent), which was spectrally cleaned by use of a cleanup filter (Laser Clean-up filter 640/10; Chroma). Emission light was filtered by a dichroic mirror (beamsplitter HC560/659; Semrock) and a band- and long-pass filter (bandpass filter HC697/75 and longpass filter LP647; Semrock) before it was projected onto an electron-multiplying charge-coupled-device camera chip (model iXon DU-897; Andor). Additional lenses in the detection path were used to generate a final pixel size of 128 nm. The equatorial plasma membrane slightly above the coverslip was imaged using a highly inclined and laminated optical sheet (Hilo). Thirty thousand images with an exposure time of 20 ms were recorded while using an irradiation intensity of ~7 kW/cm$^2$. Data were processed with the ThunderSTORM and rapidSTORM programs and analyzed with Fiji or custom-written Mathematica code. The number of CRPs in the reconstructed superresolved images with a pixel size of 20 nm was determined using the "analyze particles" command in Fiji software. LSM imaging was performed with an LSM700 system (Zeiss, Germany) equipped with a Plan-Apochromat 63× (numerical aperture, 1.4) oil objective. Cy5 fluorophores were excited with a 639-nm solid-state laser. Images were processed using LSM software Zen system 2012 and Fiji software.

**Calcium measurement.** Intracellular calcium levels were estimated using a Fluo-8 no-wash calcium assay (Abcam Ltd., Cambridge, UK). The assay was performed according to the manufacturer's protocol with minor modifications. Briefly, $1.5 \times 10^5$ cells/well were seeded in 24-well plates and allowed to plate down overnight. Prior to infection, cell culture medium was removed and the cells were washed twice with Hanks' balanced salt solution (HBSS; calcium free; Sigma). Cells were incubated with 4 $\mu$M Fluo-8 in HBSS for 30 min at 37°C in 5% $CO_2$. After incubation, the cells were washed three times with HBSS and covered with 300 $\mu$l HBSS. Fluo-8-loaded cells were then infected with bacteria in the presence or absence of 50 $\mu$M 2-APB or were left uninfected. Changes in intracellular calcium levels were observed over a 20-min period using a Nikon Eclipse Ti-E inverted microscope and evaluated with the time measurement option of Nikon NIS-Elements AR software. For analysis, individual cells were selected for single-cell analysis and tracking of calcium level changes.

**Preparation of pilus-enriched fractions.** For preparation of pilus-enriched fractions, the bacterial content of 50 blood agar plates was harvested in 40 ml of 0.15 M ethanolamine (in PBS) with a pH of 10.5. Pili were sheared off by intensive vortexing for 2 min, followed by centrifugation at 12,000 × *g* for 10 min at RT to remove the cellular debris. The supernatant was used for an additional centrifugation step at 21,000 × *g* for 90 min to remove smaller debris. Then, the supernatant was transferred to an Erlenmeyer flask, ammonium sulfate-saturated 0.15 M ethanolamine was added to a concentration of 10%, and the mixture was incubated under continuous shaking for 30 min at RT. The protein-ammonium sulfate precipitate was then harvested by centrifugation at 21,000 × *g* for 15 min. The supernatant was then discarded and the pellet was resuspended in 0.05 M Tris-buffered saline (TBS), pH 7.5. Protein solutions were then applied to a 6-ml Viva Spin column with a 7,000-dalton-molecular-weight-cutof (MWCO) and were centrifuged at 4,000 × *g* at RT until the volume reached 1 ml. To clean the sample, TBS was added again to 6 ml, followed by centrifugation as mentioned above.

**Statistical analysis.** Statistical analysis was performed with GraphPad Prism (v6) software (GraphPad Software Inc., La Jolla, CA) by an unpaired two-tailed Student's *t* test or analysis of variance (ANOVA) followed by a *post hoc* test. Significance values are indicated in the figure legends.

## SUPPLEMENTAL MATERIAL

Supplemental material for this article may be found at https://doi.org/10.1128/IAI.00410-19.

**SUPPLEMENTAL FILE 1**, PDF file, 0.1 MB.
**SUPPLEMENTAL FILE 2**, PDF file, 0.1 MB.
**SUPPLEMENTAL FILE 3**, PDF file, 0.1 MB.
**SUPPLEMENTAL FILE 4**, PDF file, 0.1 MB.
**SUPPLEMENTAL FILE 5**, PDF file, 0.1 MB.
**SUPPLEMENTAL FILE 6**, PDF file, 0.1 MB.
**SUPPLEMENTAL FILE 7**, PDF file, 0.1 MB.

## ACKNOWLEDGMENTS

We thank Lena Wolter for excellent technical help and Erhard Bieberich (Medical College of Georgia, Augusta University, GA, USA) for the rabbit IgG anticeramide

antibody. We also thank Sibylle Schneider-Schaulies for her careful reading of the manuscript.

This work was supported by Deutsche Forschungsgemeinschaft awards to A. Schubert-Unkmeir and M. Sauer (DFG SCHU 2394/2-1, SCHU 2394/2-2, and SA829/16-2).

## REFERENCES

1. Kolesnick RN, Goni FM, Alonso A. 2000. Compartmentalization of ceramide signaling: physical foundations and biological effects. J Cell Physiol 184:285–300. https://doi.org/10.1002/1097-4652(200009)184:3<285::AID-JCP2>3.0.CO;2-3.
2. Holopainen JM, Subramanian M, Kinnunen PK. 1998. Sphingomyelinase induces lipid microdomain formation in a fluid phosphatidylcholine/sphingomyelin membrane. Biochemistry 37:17562–17570. https://doi.org/10.1021/bi980915e.
3. Nurminen TA, Holopainen JM, Zhao H, Kinnunen PK. 2002. Observation of topical catalysis by sphingomyelinase coupled to microspheres. J Am Chem Soc 124:12129–12134. https://doi.org/10.1021/ja017807r.
4. Utermohlen O, Karow U, Lohler J, Kronke M. 2003. Severe impairment in early host defense against Listeria monocytogenes in mice deficient in acid sphingomyelinase. J Immunol 170:2621–2628. https://doi.org/10.4049/jimmunol.170.5.2621.
5. Grassme H, Jendrossek V, Riehle A, von Kurthy G, Berger J, Schwarz H, Weller M, Kolesnick R, Gulbins E. 2003. Host defense against Pseudomonas aeruginosa requires ceramide-rich membrane rafts. Nat Med 9:322–330. https://doi.org/10.1038/nm823.
6. Simonis A, Hebling S, Gulbins E, Schneider-Schaulies S, Schubert-Unkmeir A. 2014. Differential activation of acid sphingomyelinase and ceramide release determines invasiveness of Neisseria meningitidis into brain endothelial cells. PLoS Pathog 10:e1004160. https://doi.org/10.1371/journal.ppat.1004160.
7. Grassme H, Gulbins E, Brenner B, Ferlinz K, Sandhoff K, Harzer K, Lang F, Meyer TF. 1997. Acidic sphingomyelinase mediates entry of N. gonorrhoeae into nonphagocytic cells. Cell 91:605–615. https://doi.org/10.1016/S0092-8674(00)80448-1.
8. Esen M, Schreiner B, Jendrossek V, Lang F, Fassbender K, Grassme H, Gulbins E. 2001. Mechanisms of Staphylococcus aureus induced apoptosis of human endothelial cells. Apoptosis 6:431–439. https://doi.org/10.1023/A:1012445925628.
9. McCollister BD, Myers JT, Jones-Carson J, Voelker DR, Vázquez-Torres A. 2007. Constitutive acid sphingomyelinase enhances early and late macrophage killing of Salmonella enterica serovar Typhimurium. Infect Immun 75:5346–5352. https://doi.org/10.1128/IAI.00689-07.
10. Vazquez CL, Rodgers A, Herbst S, Coade S, Gronow A, Guzman CA, Wilson MS, Kanzaki M, Nykjaer A, Gutierrez MG. 2016. The proneurotrophin receptor sortilin is required for Mycobacterium tuberculosis control by macrophages. Sci Rep 6:29332. https://doi.org/10.1038/srep29332.
11. Teichgräber V, Ulrich M, Endlich N, Riethmüller J, Wilker B, De Oliveira-Munding CC, van Heeckeren AM, Barr ML, von Kürthy G, Schmid KW, Weller M, Tümmler B, Lang F, Grassme H, Döring G, Gulbins E. 2008. Ceramide accumulation mediates inflammation, cell death and infection susceptibility in cystic fibrosis. Nat Med 14:382–391. https://doi.org/10.1038/nm1748.
12. Zhang Y, Li X, Carpinteiro A, Gulbins E. 2008. Acid sphingomyelinase amplifies redox signaling in Pseudomonas aeruginosa-induced macrophage apoptosis. J Immunol 181:4247–4254. https://doi.org/10.4049/jimmunol.181.6.4247.
13. Zhang Y, Li X, Grassme H, Doring G, Gulbins E. 2010. Alterations in ceramide concentration and pH determine the release of reactive oxygen species by Cftr-deficient macrophages on infection. J Immunol 184:5104–5111. https://doi.org/10.4049/jimmunol.0902851.
14. Yu H, Zeidan YH, Wu BX, Jenkins RW, Flotte TR, Hannun YA, Virella-Lowell I. 2009. Defective acid sphingomyelinase pathway with Pseudomonas aeruginosa infection in cystic fibrosis. Am J Respir Cell Mol Biol 41:367–375. https://doi.org/10.1165/rcmb.2008-0295OC.
15. Nakatsuji T, Tang DC, Zhang L, Gallo RL, Huang CM. 2011. Propionibacterium acnes CAMP factor and host acid sphingomyelinase contribute to bacterial virulence: potential targets for inflammatory acne treatment. PLoS One 6:e14797. https://doi.org/10.1371/journal.pone.0014797.
16. Hauck CR, Grassme H, Bock J, Jendrossek V, Ferlinz K, Meyer TF, Gulbins E. 2000. Acid sphingomyelinase is involved in CEACAM receptor-mediated phagocytosis of Neisseria gonorrhoeae. FEBS Lett 478:260–266. https://doi.org/10.1016/S0014-5793(00)01851-2.
17. Schramm M, Herz J, Haas A, Kronke M, Utermohlen O. 2008. Acid sphingomyelinase is required for efficient phago-lysosomal fusion. Cell Microbiol 10:1839–1853. https://doi.org/10.1111/j.1462-5822.2008.01169.x.
18. Peng H, Li C, Kadow S, Henry BD, Steinmann J, Becker KA, Riehle A, Beckmann N, Wilker B, Li PL, Pritts T, Edwards MJ, Zhang Y, Gulbins E, Grassme H. 2015. Acid sphingomyelinase inhibition protects mice from lung edema and lethal Staphylococcus aureus sepsis. J Mol Med (Berl) 93:675–689. https://doi.org/10.1007/s00109-014-1246-y.
19. Kornhuber J, Rhein C, Muller CP, Muhle C. 2015. Secretory sphingomyelinase in health and disease. Biol Chem 396:707–736. https://doi.org/10.1515/hsz-2015-0109.
20. Zeidan YH, Hannun YA. 2007. Activation of acid sphingomyelinase by protein kinase Cdelta-mediated phosphorylation. J Biol Chem 282:11549–11561. https://doi.org/10.1074/jbc.M609424200.
21. Zeidan YH, Wu BX, Jenkins RW, Obeid LM, Hannun YA. 2008. A novel role for protein kinase Cdelta-mediated phosphorylation of acid sphingomyelinase in UV light-induced mitochondrial injury. FASEB J 22:183–193. https://doi.org/10.1096/fj.07-8967com.
22. Li X, Gulbins E, Zhang Y. 2012. Oxidative stress triggers Ca-dependent lysosome trafficking and activation of acid sphingomyelinase. Cell Physiol Biochem 30:815–826. https://doi.org/10.1159/000341460.
23. Andrews NW, Almeida PE, Corrotte M. 2014. Damage control: cellular mechanisms of plasma membrane repair. Trends Cell Biol 24:734–742. https://doi.org/10.1016/j.tcb.2014.07.008.
24. Caugant DA, Maiden MCJ. 2009. Meningococcal carriage and disease—population biology and evolution. Vaccine 27(Suppl 2):B64–B70. https://doi.org/10.1016/j.vaccine.2009.04.061.
25. Cartwright KA, Stuart JM, Jones DM, Noah ND. 1987. The Stonehouse survey: nasopharyngeal carriage of meningococci and Neisseria lactamica. Epidemiol Infect 99:591–601. https://doi.org/10.1017/s0950268800066449.
26. Virji M, Saunders JR, Sims G, Makepeace K, Maskell D, Ferguson DJ. 1993. Pilus-facilitated adherence of Neisseria meningitidis to human epithelial and endothelial cells: modulation of adherence phenotype occurs concurrently with changes in primary amino acid sequence and the glycosylation status of pilin. Mol Microbiol 10:1013–1028. https://doi.org/10.1111/j.1365-2958.1993.tb00972.x.
27. Nassif X, Beretti JL, Lowy J, Stenberg P, O'Gaora P, Pfeifer J, Normark S, So M. 1994. Roles of pilin and PilC in adhesion of Neisseria meningitidis to human epithelial and endothelial cells. Proc Natl Acad Sci U S A 91:3769–3773. https://doi.org/10.1073/pnas.91.9.3769.
28. Helaine S, Carbonnelle E, Prouvensier L, Beretti JL, Nassif X, Pelicic V. 2005. PilX, a pilus-associated protein essential for bacterial aggregation, is a key to pilus-facilitated attachment of Neisseria meningitidis to human cells. Mol Microbiol 55:65–77. https://doi.org/10.1111/j.1365-2958.2004.04372.x.
29. Carbonnelle E, Helaine S, Nassif X, Pelicic V. 2006. A systematic genetic analysis in Neisseria meningitidis defines the Pil proteins required for assembly, functionality, stabilization and export of type IV pili. Mol Microbiol 61:1510–1522. https://doi.org/10.1111/j.1365-2958.2006.05341.x.
30. Cehovin A, Simpson PJ, McDowell MA, Brown DR, Noschese R, Pallett M, Brady J, Baldwin GS, Lea SM, Matthews SJ, Pelicic V. 2013. Specific DNA recognition mediated by a type IV pilin. Proc Natl Acad Sci U S A 110:3065–3070. https://doi.org/10.1073/pnas.1218832110.
31. Tonjum T, Freitag NE, Namork E, Koomey M. 1995. Identification and characterization of pilG, a highly conserved pilus-assembly gene in pathogenic Neisseria. Mol Microbiol 16:451–464. https://doi.org/10.1111/j.1365-2958.1995.tb02410.x.
32. Merz AJ, So M, Sheetz MP. 2000. Pilus retraction powers bacterial twitching motility. Nature 407:98–102. https://doi.org/10.1038/35024105.
33. Fussenegger M, Rudel T, Barten R, Ryll R, Meyer TF. 1997. Transformation competence and type-4 pilus biogenesis in Neisseria gonorrhoeae—a review. Gene 192:125–134. https://doi.org/10.1016/S0378-1119(97)00038-3.
34. Hoffmann I, Eugene E, Nassif X, Couraud PO, Bourdoulous S. 2001.

Activation of ErbB2 receptor tyrosine kinase supports invasion of endothelial cells by Neisseria meningitidis. J Cell Biol 155:133–143. https://doi.org/10.1083/jcb.200106148.
35. Kallstrom H, Islam MS, Berggren PO, Jonsson AB. 1998. Cell signaling by the type IV pili of pathogenic Neisseria. J Biol Chem 273:21777–21782. https://doi.org/10.1074/jbc.273.34.21777.
36. Ayala BP, Vasquez B, Clary S, Tainer JA, Rodland K, So M. 2001. The pilus-induced $Ca^{2+}$ flux triggers lysosome exocytosis and increases the amount of Lamp1 accessible to Neisseria IgA1 protease. Cell Microbiol 3:265–275. https://doi.org/10.1046/j.1462-5822.2001.00112.x.
37. Nassif X, Lowy J, Stenberg P, O'Gaora P, Ganji A, So M. 1993. Antigenic variation of pilin regulates adhesion of Neisseria meningitidis to human epithelial cells. Mol Microbiol 8:719–725. https://doi.org/10.1111/j.1365-2958.1993.tb01615.x.
38. Asmat TM, Tenenbaum T, Jonsson AB, Schwerk C, Schroten H. 2014. Impact of calcium signaling during infection of Neisseria meningitidis to human brain microvascular endothelial cells. PLoS One 9:e114474. https://doi.org/10.1371/journal.pone.0114474.
39. Morand PC, Drab M, Rajalingam K, Nassif X, Meyer TF. 2009. Neisseria meningitidis differentially controls host cell motility through PilC1 and PilC2 components of type IV pili. PLoS One 4:e6834. https://doi.org/10.1371/journal.pone.0006834.
40. Heilemann M, van de Linde S, Schuttpelz M, Kasper R, Seefeldt B, Mukherjee A, Tinnefeld P, Sauer M. 2008. Subdiffraction-resolution fluorescence imaging with conventional fluorescent probes. Angew Chem Int Ed 47:6172–6176. https://doi.org/10.1002/anie.200802376.
41. Burgert A, Schlegel J, Becam J, Doose S, Bieberich E, Schubert-Unkmeir A, Sauer M. 2017. Characterization of plasma membrane ceramides by super-resolution microscopy. Angew Chem Int Ed 56:6131–6135. https://doi.org/10.1002/anie.201700570.
42. Bernard SC, Simpson N, Join-Lambert O, Federici C, Laran-Chich MP, Maissa N, Bouzinba-Segard H, Morand PC, Chretien F, Taouji S, Chevet E, Janel S, Lafont F, Coureuil M, Segura A, Niedergang F, Marullo S, Couraud PO, Nassif X, Bourdoulous S. 2014. Pathogenic Neisseria meningitidis utilizes CD147 for vascular colonization. Nat Med 20:725–731. https://doi.org/10.1038/nm.3563.
43. Grassme H, Henry B, Ziobro R, Becker KA, Riethmuller J, Gardner A, Seitz AP, Steinmann J, Lang S, Ward C, Schuchman EH, Caldwell CC, Kamler M, Edwards MJ, Brodlie M, Gulbins E. 2017. $\beta$1-Integrin accumulates in cystic fibrosis luminal airway epithelial membranes and decreases sphingosine, promoting bacterial infections. Cell Host Microbe 21:707–718.e8. https://doi.org/10.1016/j.chom.2017.05.001.
44. Ayala P, Wilbur JS, Wetzler LM, Tainer JA, Snyder A, So M. 2005. The pilus and porin of Neisseria gonorrhoeae cooperatively induce Ca(2+) transients in infected epithelial cells. Cell Microbiol 7:1736–1748. https://doi.org/10.1111/j.1462-5822.2005.00586.x.
45. Ayala P, Vasquez B, Wetzler L, So M. 2002. Neisseria gonorrhoeae porin P1.B induces endosome exocytosis and a redistribution of Lamp1 to the plasma membrane. Infect Immun 70:5965–5971. https://doi.org/10.1128/IAI.70.11.5965-5971.2002.
46. Muller A, Gunther D, Dux F, Naumann M, Meyer TF, Rudel T. 1999. Neisserial porin (PorB) causes rapid calcium influx in target cells and induces apoptosis by the activation of cysteine proteases. EMBO J 18:339–352. https://doi.org/10.1093/emboj/18.2.339.
47. Reference deleted.
48. Reference deleted.
49. Berridge MJ, Lipp P, Bootman MD. 2000. The versatility and universality of calcium signalling. Nat Rev Mol Cell Biol 1:11–21. https://doi.org/10.1038/35036035.
50. Carafoli E, Santella L, Branca D, Brini M. 2001. Generation, control, and processing of cellular calcium signals. Crit Rev Biochem Mol Biol 36:107–260. https://doi.org/10.1080/20014091074183.
51. Lin L, Ayala P, Larson J, Mulks M, Fukuda M, Carlsson SR, Enns C, So M. 1997. The Neisseria type 2 IgA1 protease cleaves LAMP1 and promotes survival of bacteria within epithelial cells. Mol Microbiol 24:1083–1094. https://doi.org/10.1046/j.1365-2958.1997.4191776.x.
52. Jaiswal JK, Andrews NW, Simon SM. 2002. Membrane proximal lysosomes are the major vesicles responsible for calcium-dependent exocytosis in nonsecretory cells. J Cell Biol 159:625–635. https://doi.org/10.1083/jcb.200208154.
53. Reddy A, Caler EV, Andrews NW. 2001. Plasma membrane repair is mediated by Ca(2+)-regulated exocytosis of lysosomes. Cell 106:157–169. https://doi.org/10.1016/S0092-8674(01)00421-4.
54. Rodriguez A, Webster P, Ortego J, Andrews NW. 1997. Lysosomes behave as $Ca^{2+}$-regulated exocytic vesicles in fibroblasts and epithelial cells. J Cell Biol 137:93–104. https://doi.org/10.1083/jcb.137.1.93.
55. Fernandes MC, Cortez M, Flannery AR, Tam C, Mortara RA, Andrews NW. 2011. Trypanosoma cruzi subverts the sphingomyelinase-mediated plasma membrane repair pathway for cell invasion. J Exp Med 208:909–921. https://doi.org/10.1084/jem.20102518.
56. Luisoni S, Suomalainen M, Boucke K, Tanner LB, Wenk MR, Guan XL, Grzybek M, Coskun U, Greber UF. 2015. Co-option of membrane wounding enables virus penetration into cells. Cell Host Microbe 18:75–85. https://doi.org/10.1016/j.chom.2015.06.006.
57. Charruyer A, Grazide S, Bezombes C, Muller S, Laurent G, Jaffrezou JP. 2005. UV-C light induces raft-associated acid sphingomyelinase and JNK activation and translocation independently on a nuclear signal. J Biol Chem 280:19196–19204. https://doi.org/10.1074/jbc.M412867200.
58. Dumitru CA, Carpinteiro A, Trarbach T, Hengge UR, Gulbins E. 2007. Doxorubicin enhances TRAIL-induced cell death via ceramide-enriched membrane platforms. Apoptosis 12:1533–1541. https://doi.org/10.1007/s10495-007-0081-9.
59. Grassme H, Jekle A, Riehle A, Schwarz H, Berger J, Sandhoff K, Kolesnick R, Gulbins E. 2001. CD95 signaling via ceramide-rich membrane rafts. J Biol Chem 276:20589–20596. https://doi.org/10.1074/jbc.M101207200.
60. Grassme H, Riehle A, Wilker B, Gulbins E. 2005. Rhinoviruses infect human epithelial cells via ceramide-enriched membrane platforms. J Biol Chem 280:26256–26262. https://doi.org/10.1074/jbc.M500835200.
61. Avota E, Gulbins E, Schneider-Schaulies S. 2011. DC-SIGN mediated sphingomyelinase-activation and ceramide generation is essential for enhancement of viral uptake in dendritic cells. PLoS Pathog 7:e1001290. https://doi.org/10.1371/journal.ppat.1001290.
62. Stins MF, Gilles F, Kim KS. 1997. Selective expression of adhesion molecules on human brain microvascular endothelial cells. J Neuroimmunol 76:81–90. https://doi.org/10.1016/S0165-5728(97)00036-2.
63. Unkmeir A, Latsch K, Dietrich G, Wintermeyer E, Schinke B, Schwender S, Kim KS, Eigenthaler M, Frosch M. 2002. Fibronectin mediates Opc-dependent internalization of Neisseria meningitidis in human brain microvascular endothelial cells. Mol Microbiol 46:933–946. https://doi.org/10.1046/j.1365-2958.2002.03222.x.
64. Lappann M, Haagensen JA, Claus H, Vogel U, Molin S. 2006. Meningococcal biofilm formation: structure, development and phenotypes in a standardized continuous flow system. Mol Microbiol 62:1292–1309. https://doi.org/10.1111/j.1365-2958.2006.05448.x.
65. Reference deleted.
66. Virji M, Heckels JE. 1983. Antigenic cross-reactivity of Neisseria pili: investigations with type- and species-specific monoclonal antibodies. J Gen Microbiol 129:2761–2768. https://doi.org/10.1099/00221287-129-9-2761.